Acta Astronautica 158 (2019) 438–443

Contents lists available at ScienceDirect

Acta Astronautica

journal homepage: www.elsevier.com/locate/actaastro

Evaluation of the grid convergence for a rocket combustion chamber with a porous injector

Victor P. Zhukov*, Klaus P. Heinrich

Institute of Space Propulsion, German Aerospace Center (DLR), Langer Grund, 74239, Hardthausen, Germany

ARTICLE INFO

Keywords:
Computational fluid dynamics
Grid convergence
Porous injector
Liquid rocket engine
Cryogenic fuels

ABSTRACT

A study of the grid convergence was carried out in order to quantify the mesh impact on simulations of rocket combustion chambers performed using the averaged Navier–Stokes equations. The present work is a continuation of previous studies on simulations of rocket combustion chambers with the porous injector head API-68. Turbulence is modelled by the SST turbulence model; turbulent combustion is modelled using the extended eddy-dissipation model. The grid convergence study is carried out for two injector configurations (one injector in the middle of the injector head and one injector near the sidewall) on five meshes for each configuration. Results of the work show that the dependences of the flame length and wall heat flux on mesh spacing are described well by a parabola. Using the found dependence on mesh spacing, spatial discretization errors have been evaluated. Analysis of the results shows that a reasonable accuracy of modelling can be reached using the current computational fluid dynamic model at a mesh spacing of around 30 μm in the flame area.

1. Introduction

The current situation on the space launch market, the pricing pressure from private spaceflight companies, and a desire to reduce cost from government space agencies has established new requirements for rocket engines. Nowadays, rocket engines should be cost-effective. This does not mean that rocket engines should be cheap as this in turn can increase other costs, but they should be a part of a cost-effective service for cargo delivery to orbit. One of the developments aimed at cost reduction is an Advanced Porous Injector (API). This is a concept of an injector head for rocket engines, which has been under development at the German Aerospace Center (DLR-Lampoldshausen) for the last decade [1]. Advanced porous injectors allow reducing manufacturing costs while achieving a better performance. In API injector, fuel is fed into the combustion chamber through a porous plate; oxidizer is fed through many small injectors uniformly distributed over the injector plate similar to a showerhead, see Fig. 1.

Thermal management is a key problem of rocket engine design. In recent work, Zhukov and Suslov studied wall heat fluxes in a combustion chamber with the injector API-68 carrying out hot-run tests and fluid simulations [2]. Computational Fluid Dynamics (CFD) simulations are another way of reducing cost during the development phase. The comparison of the results of work [2] with the results of the previous attempts to simulate the flow in the combustion chamber with API-68 [3] shows that there is a visible impact of numerical grid spacing on the simulation results. The numerical mesh increased from 2.6 Mio cells in the first simulations to 6.2 Mio cells in the final simulations [2]. At the same time, the flame grew in length from 3 cm to 5 cm. However, during the continuous work it was found that a further increase of the mesh size does not lead to significant changes in the results [2]. Nevertheless, the problem of the quantitative characterization of the mesh effect was not solved in work [2], and it is still an issue. The aim of the present work is the quantification of the grid convergence and the evaluation of the numerical error associated with spatial discretization.

First, it is necessary to say a few words about the object of the research. The main element of the injector API-68 is a porous plate sintered from bronze beads with a diameter of about 0.6 mm. This plate is permeated by 68 stainless steel tubes of small diameter, which are practically uniformly distributed over the porous plate, see Fig. 1. These tubes are the oxygen injectors. They have a plain geometry and a sharp cut (no tapering nor recess). The oxygen injectors have an outer diameter of 2 mm and an inner diameter of 1.5 mm (this value was incorrectly given in Table 3 of previous article [2]). Hydrogen is fed uniformly through the porous plate. Other images of API-68 can be found in [1–4]. API-68 demonstrated a high combustion efficiency in a wide range of parameters: chamber pressure, injection temperature, and mass flow rates [1].

The combustion chamber used in [2,3] is a cylindrical copper

* Corresponding author.
E-mail address: victor.zhukov@dlr.de (V.P. Zhukov).

https://doi.org/10.1016/j.actaastro.2018.08.002
Received 9 February 2018; Received in revised form 4 May 2018; Accepted 1 August 2018
Available online 08 August 2018

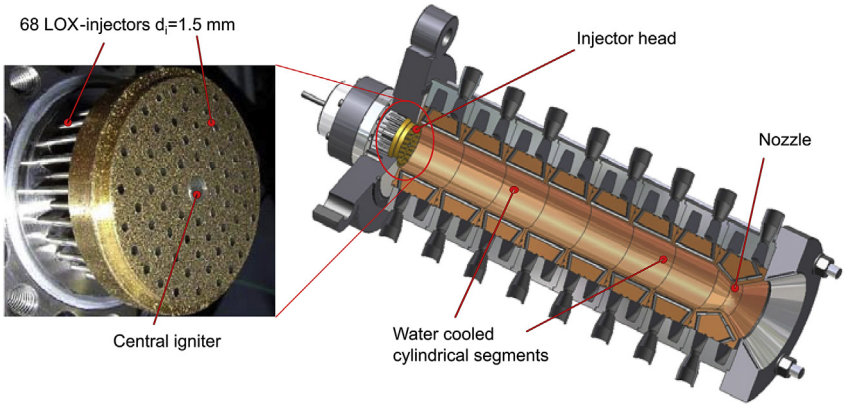

Fig. 1. A photo of the porous injector head API-68 and the cross-section of the calorimetric combustion chamber [2].

calorimetric chamber with a diameter of 50 mm and consists of separate segments. The segments allow measuring wall temperature, wall heat flux, and static pressure along the chamber axis with a spatial resolution of 50 mm.

2. Modelling

The flow in the studied combustion chamber is very nonuniform. The grid resolution plays an important role only in areas of high gradients. Therefore, there is no need to perform a grid convergence study for the whole combustion chamber. The region, where the mesh effect was observed, is only in the vicinity of the flame. Here are the highest gradients of pressure, density, velocity, and mass fractions.

In API-68 the 68 oxygen injectors are aligned in a rectangular pattern, see Fig. 1. Therefore, only one eighth of the combustion chamber, a sector of 45°, was modelled to save computational time in [2]. Here, in order to reduce the computational cost further, the simulations are reduced to two separate oxygen injectors. The injectors chosen for the present study are shown in Fig. 2 as Injector I and Injector II. Injector I was chosen because it can be represented in a very simple domain and is surrounded from all sides by other injectors. All of its sidewalls can be considered as symmetry planes. Injector II is located closer to the sidewall than other injectors, so it has the largest impact on wall heat flux. The numerical domains of Injectors I and II have also the upstream part of oxygen injector. It is a plain cylindrical tube with an inner diameter of 1.5 mm and a length of 15 mm located upstream of the injector plate. A part of oxygen injector is needed to form a realistic exit velocity profile with the boundary layer on the wall.

In the present study, the same physical model and numerical setup are used as in our previous work [2], where their detailed description can be found. The main points of the numerical model, which directly affect the results of the present study, are given below. The flow is modelled using the Favre-averaged Navier–Stokes equations. The simulations have been performed using the commercial CFD code ANSYS CFX [5]. All governing equations excluding the equations for enthalpy and for mass fractions of mixture components have been solved using "High Resolution" advection scheme [5]. The order of the advection scheme reduces to the first order near discontinuities and is as close as possible to the second order without violating the boundedness principle [6]. The transport equations for enthalpy and for the mass fractions of mixture components have been solved using the first order upwind differencing scheme. The first order scheme has been used because of divergence in the solver during use of the high resolution scheme. The reason of the divergence is numerical dispersion due to high gradients of temperature and mass fractions.

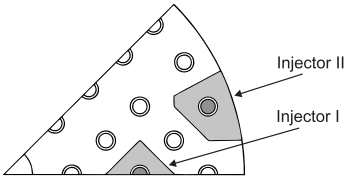

Fig. 2. Arrangement of oxygen injectors in API-68 (45° sector).

Turbulence has been modelled using the SST $k-\omega$ turbulence model [5]. Turbulent combustion has been modelled using the extended eddy-dissipation model. In this model, the degree of the chemical reaction is regulated by a special parameter called "Maximum flame temperature". This tabulated parameter sets the temperature of burnt gases in correspondence with the local mass ratio of oxygen atoms to hydrogen atoms in the mixture. (This ratio oxygen-to-hydrogen plays a role similar to equivalence ratio.) Flame temperatures are calculated using the program NASA Chemical Equilibrium with Applications (CEA) by [7]. One can find other details of the numerical model in our recent works [2,8,9].

Finally, it is necessary to give a brief description of applied boundary conditions. Oxygen is fed through the tube in the middle of the domains; hydrogen is fed through the surface of the injector plate. They are separated by a small ring (injector tip), which has a thickness of 0.25 mm. Fig. 3 gives an overall picture of the arrangement of boundary conditions. Propellants are injected at cryogenic temperatures and with velocities which are calculated based on the assumption that propellants are uniformly distributed over the cross-section of the injector head. The values of temperatures and mass flow rates as well as other boundary conditions have been taken from work [2] and are presented in Table 1. At the outlet, the pressure has been set; in the case of Injector I, all sidewalls are symmetry planes.

3. Grid convergence study

The mesh effect manifested itself in an elongation of the flame, see Fig. 3. The flame becomes slightly longer with the mesh refinement

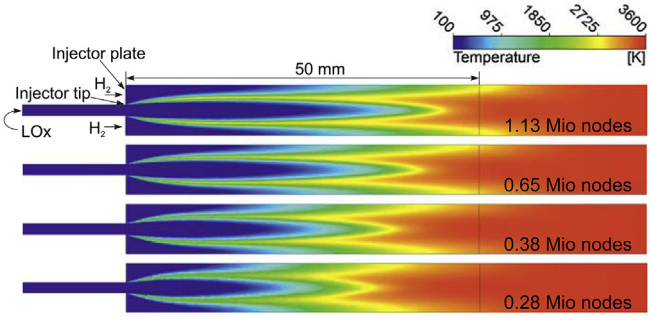

Fig. 3. Flame of Injector I at four different mesh densities.

Table 1
Boundary conditions for the simulation according to [2].

Injection velocity, O_2	13.56 m/s
Temperature, O_2	120 K
Injection velocity, H_2	9.10 m/s
Temperature, H_2	100 K
Mass ratio of oxidizer-to-fuel (ROF)	6[a]
Pressure at the outlet	~75.5 bar

[a] Average value for the combustion chamber.

without changing its shape and other characteristics. The aim of the present work is to quantify the grid convergence for the case of the combustion chamber with the porous injector API-68. The mesh from previous work [2] was taken as a baseline mesh. This unstructured mesh consists of tetrahedral elements with prism layers on the walls. The mesh is uniform with the average spacing (a distance between nodes) equal to 150 µm. The mesh has prism layers near the sidewalls and around the oxygen posts (walls which separate oxygen from hydrogen). The spacing at the tip of the oxygen post amounts to about 18 µm. The thickness of the first prism layer equals to 4 µm. This corresponds to a value of y^+ (non-dimensional wall distance) of about 11. A further refinement of the mesh near the walls makes no sense because the walls are considered to be rough and the thickness of the first prism layer would be notably less than the roughness of the walls which is set equal to 5 µm.

The grid convergence study was carried out using five grids for both Injector I and II. Two of the five meshes have higher grid densities than the baseline mesh, and the other two meshes have lower grid densities. The refinement factor for the spacing is the same for all directions and equals to 1.26; the coarsening factor equals to 1/1.26, respectively. One of the challenges, which researchers are faced with during grid convergence studies, is that the number of nodes in the numerical mesh grows very fast during mesh refinement especially in three-dimensional (3D) cases. The typical refinement factor of 2 means the increase of node number by eight times during mesh refinement. In the present work, a refinement factor of $1.26 = \sqrt[3]{2}$ doubles the amount of nodes in one refinement step. Often, simulations are carried out on meshes which are near to the limit of available computational resources; thus, a further refinement is impossible. On the other hand, the coarsening of mesh is also often not possible because a coarse mesh may give physically incorrect results. For this reason, the most coarse mesh in Table 2 is not twice smaller as Mesh II. The cells near walls, at inlets, and at outlets can be coarsened only to some extend. Injector I has the simplest configuration among the oxygen injectors; thus, the effect of the walls and of the boundary conditions is minimal. This argument played a role in the choice of Injector I.

4. Results and discussion

4.1. Injector I

The results of the grid convergence study for Injector I are gathered in Table 2 for ease of reference. As the previous works, the flame length depends on the mesh density, see Fig. 3. The parameters of gas in the post-flame zone (temperatures, pressures, densities, mass fractions, etc.) do not show any sensitivity to the mesh density. In the present case, the flame length is a convenient parameter for the quantification of the grid convergence. First, the flame length has shown a higher sensitivity to the mesh density than other parameters of gas and flow. Secondly, it can be easily interpreted and measured. In our case, the flame length is defined as a distance from the injector plate to a point where the temperature on the axis of the injector reaches 2000 K, which corresponds to the colour between green and yellow in Fig. 3.

Table 2
Grid convergence study, Injector I.

Meshes	I	II	III	IV	V
Spacing (µm)	238	189	150	119	95
Nodes (Mio[a])	0.28	0.38	0.65	1.13	2.03
Flame length (mm)	30.2	34.0	38.3	42.1	47.0
Normalized h	1.59	1.26	1.00	0.79	0.63

[a] 1 Mio = 10^6.

The flame front and boundary layers are objects with the smallest thicknesses in rocket combustion chambers. While the resolution of boundary layers is a solvable problem, the resolution of the flame front is a very complex task, especially in case of rocket combustion chambers. Flame fronts are very thin at high pressures. The thickness of laminar hydrogen–oxygen flames amounts to 100–200 µm at pressures of 50–100 bar [10]. In our simulations, the turbulent flame has a similar thickness near the oxygen injector. In contrast to boundary layers, the flame does not have a predetermined position in the combustion chamber, so it is necessary to fill a relatively large volume of the combustion chamber with a very fine mesh. When a mesh is too coarse for the flame front, errors occur in the evaluation of both mass fractions and their gradients at the integration point. The use of a coarse mesh in combination with low-order advection schemes increases the impact of numerical dissipation which in turn results in the reduction of the flame length.

In Fig. 4, one can see the dependence of the flame length on mesh spacing. The numerical model uses both first and second order advection schemes, and therefore the results are approximated by a mixed-order equation:

$$F(h) = F_{exact} + C_1 h + C_2 h^2 + \mathcal{O}(h^3) \quad (1)$$

where F is flame length, h is mesh spacing, and $F_{exact} := F(h \to 0)$. Here we assume that the numerical solution converges to the exact solution. Neglecting the third-order terms, we get

$$F(h) = F_{exact} + C_1 h + C_2 h^2 \quad (2)$$

The idea to use the mixed order equation came from the work by Roy who carried out a detailed analysis of grid convergence errors in the case of mixed-order numerical schemes [11]. As we can see in Fig. 4, the dependence of the flame length on spacing is described by a parabola (Eq. (2)) very well.

Using Eq. (2) we can evaluate a spatial discretization error:

$$\frac{F_{exact} - F(h)}{F_{exact}} \times 100\%$$

In Fig. 5 one can see the spatial errors in the flame length for

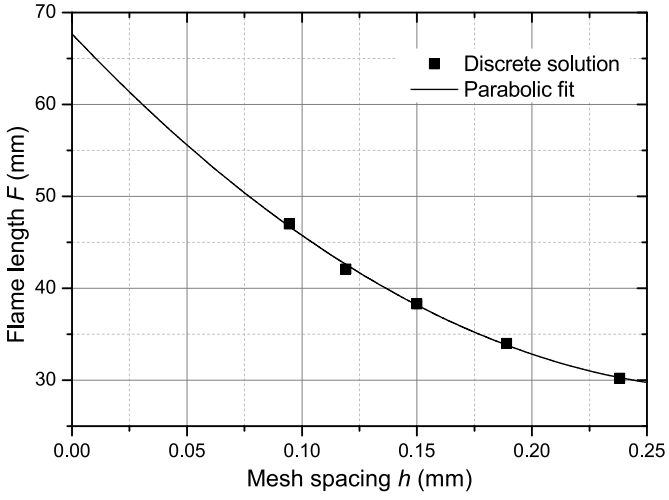

Fig. 4. Flame length F as a function of mesh spacing h.

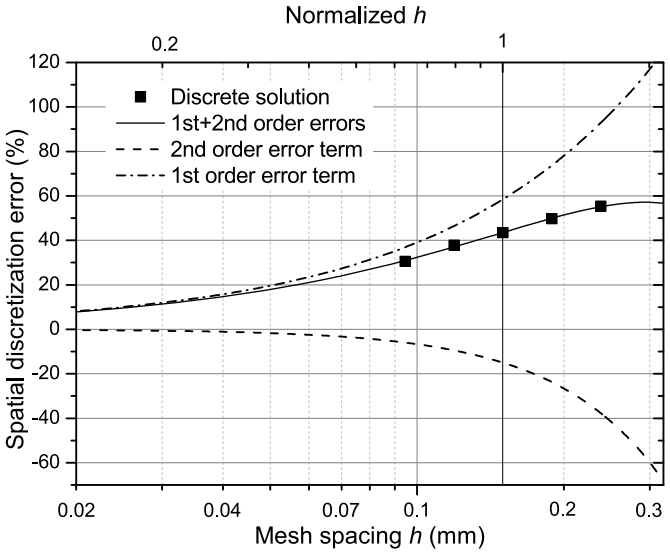

Fig. 5. Spatial discretization error in the flame length as a function of mesh spacing h.

different meshes. The graph also shows the first- and second-order error terms (100 %× $C_1 h/F_{exact}$ and 100 %× $C_2 h^2/F_{exact}$) along with their sum.

First, one may notice that the spatial discretization error in the flame length for the tested meshes reaches relatively high values of 30–60%. An acceptable value of the spatial error is reached at a mesh spacing of several tens of microns. The second order term rapidly declines with mesh spacing, and below 0.1 mm the spatial convergence actually has the first order. This result is not surprising because the transport equation for mass fractions, which plays a major role in this case, is discretized using the first-order advection scheme.

The difference in the magnitudes of the first- and second-order error terms at $h = 0.1$ mm emphasizes the advantages of second-order schemes in comparison with first-order schemes. Additionally, the first- and second-order error terms have different signs. At $h \approx 0.6$ mm, the flame length theoretically may reach the exact value of 67.7 mm (if we will prolongate the solid line outside the graph, it will cross the horizontal axis at $h \approx 0.6$ mm). However, spatial discretization errors for other parameters (p, T, ρ, v_i , etc.) may be very large on such coarse meshes. Indeed, the constants C_1 and C_2 in Eq. (1) have individual values for each parameter. While only the increase of the flame length has been observed during this mesh study, the numerical solution may be completely different on a much coarser mesh with a spacing of 0.6 mm.

4.2. Injector II

The case of Injector II is more important than the previous case because the major goal of CFD simulations of rocket combustion chambers is the prediction of the heat transfer to the walls. For the thermal loads on walls, the outer row of injectors has the largest impact while Injector II makes the biggest contribution. The same numerical model as for Injector I has been used for Injector II in the simulations. The difference between the configurations is that one side of the numerical domain of Injector II has been treated as a no-slip isothermal wall. The sidewall has been divided into five segments of 50 mm length, where each segment has a temperature in accordance with the measurements [2]. The roughness of walls has been set to 5 μm. A view of Injector II with temperature fields in the longitudinal section and on the sidewall is shown in Fig. 6.

Here we are looking at the grid convergence for wall heat flux instead of flame length because wall heat flux is the main goal of our CFD simulations. Regarding the flame length in the case of Injector II, it has the same dependence on the mesh refinement as in the case of Injector I.

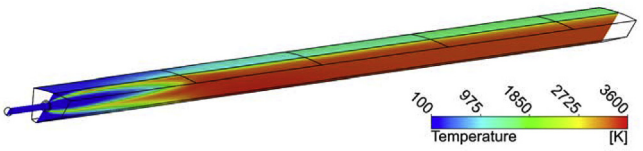

Fig. 6. Simulation of Injector II, temperature fields in the longitudinal section and on the sidewall.

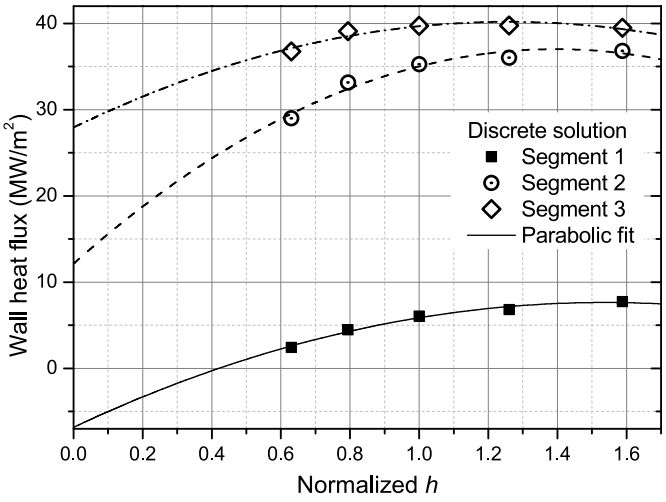

Fig. 7. Wall heat flux in Segments 1, 2 and 3 as a function of mesh spacing h.

The flame of Injector II is bent towards the wall and also depends on the flow in the wall boundary layer. Thus, Injector I is more convenient to evaluate the mesh effect on the flame length.

The dependences of the wall heat fluxes on mesh spacing are shown in Figs. 7 and 8. Here wall heat flux is an average value of heat flux on each segment, i.e. the average wall heat flux for each 50 mm in the longitudinal direction. The experimental values cannot be plotted here because the simulations do not include the three other outer oxygen injectors. The simulated wall heat flux depends mainly on the spacing in the prism layers, where spacing varies from layer to layer. Therefore, the curves are plotted against a normalized mesh spacing. The dependence of the wall heat flux on grid spacing is also well described by a parabola (i.e. by Eq. (2)). The influence of grid spacing (in absolute values) is maximum for Segment 2, which covers the distances from the injector plate from 50 mm to 100 mm. Further downstream, the impact

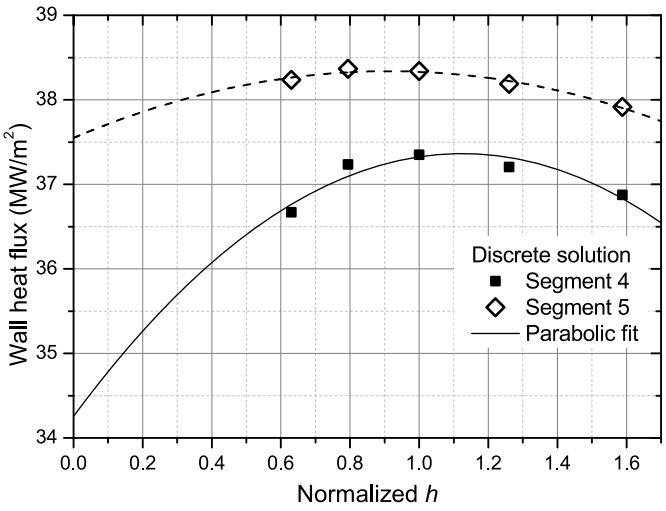

Fig. 8. Wall heat flux in Segments 4 and 5 as a function of mesh spacing h.

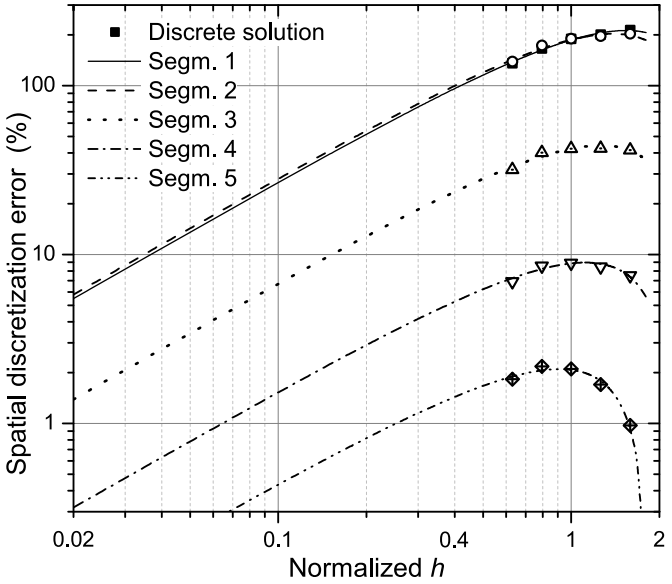

Fig. 9. Spatial discretization error in the wall heat flux as a function of mesh spacing h.

of spacing decreases with the distance from the injector plate. It is worth noting that the graph in Fig. 8 has a significantly smaller chart scale on the vertical axis than the scale in Fig. 7.

Using the same method as in the previous section, we have calculated the spatial discretization error in the wall heat flux. The results of the calculations have been compiled in one chart, see Fig. 9. The chart clearly shows that the impact of the mesh decreases with the distance from the injector plate and that the largest effect is observed for Segments 1 and 2. Such dependence of the discretization error on axial coordinate is not surprising. For the tested meshes, the flame length varies from 30 to 50 mm. Hot gases reach the sidewall around 10 mm further downstream, so the distance, at which the hot gases make contact with the sidewall, varies from 40 to 60 mm for different mesh spacings. Meanwhile, the border between Segments 1 and 2 is located at $x = 50$ mm, so the flame crosses the border of the segments. Behind the flame front, the temperature of hot gases is relatively constant; therefore, the mesh impact on the wall heat flux and on the flow is low at large distances from the injector plate.

4.3. Discussion

Equation (2), which has been used to describe the mesh effect, has a mixed order. This leads to two important consequences. The first consequence is that the order of mesh convergence is virtually defined by lower-order terms in the case of mixed order. The higher-order term becomes smaller than the lower-order term as spacing h tends to zero, which is shown in Fig. 5. The second consequence is that first- and second-order terms may have a different sign and compensate each other at a certain value of h. For a grid convergence study with a small number of meshes, this may look like a grid divergence or as an apparent independence of the simulation from mesh density. Equation (2) has three independent parameters; therefore, it is necessary to use at least four meshes in order to evaluate the order of grid convergence reliably, the level of spatial discretization error, and the current position on the parabola. If a grid convergence study is carried out with a small refinement factor, i.e. the mesh spacing is varied in a narrow range, and the spatial discretization error amounts to a few tens of percent, it may result in a large error of $F_{exact} = F(h \to 0)$. In such cases, it is necessary to use more than four meshes.

The transition from the mixed order to the second order is unlikely possible in simulations of rocket combustion chambers due to strong gradients of temperature, density, and species concentrations in flame. According to work [10], the laminar flame front thickness amounts to about 100 μm at the studied conditions while parameters of gas (temperature, density, etc.) change their value by orders of magnitude within the flame front. In the simulations the flame thickness is significantly larger; the flame is turbulent, and its thickness depends on the model parameters. However, the simulated flame is much thinner than 1 mm. The second-order advection schemes generate wiggles (or oscillations) near gradients, which is called numerical dispersion. This is the reason why the first-order upwind scheme is used for the transport equations for H and Y_i (enthalpy and mass fractions), and for other variables (ρ, v_i , k, and ω) the "High Resolution" scheme is used which reduces from the second order to the first order near discontinuities. As a consequence, the obtained numerical solution is characterized by a mixed-order accuracy in mesh spacing.

With regard to the particular case considered here, the spatial discretization error of the wall heat flux reaches very high values for Segments 1 and 2, see Fig. 9. In the case of Injector I (see Fig. 5), the model underpredicts the flame length with an error of 10% at $h = 30$ μm, whereas this spacing still corresponds an error of 50% in the wall heat flux for Segments 1 and 2. This large error cannot be explained solely by the increase of the flame length due to the mesh refinement and by passing the flame over the border of these segments. There is also a second reason for the large value of the spatial discretization error of the wall heat flux. In contrast to the domain of Injector I, the domain of Injector II has the sidewall and the region where the flame makes contact with the sidewall, i.e. the flame penetrates into the boundary layer. The large value of the error results from the relatively large cells in this region, where the flame interacts with the boundary layer. To obtain a solution with a small discretization error for Injector II, it is necessary to use a mesh with another distribution of nodes, i.e. a finer mesh in the region where the flame interacts with the boundary layer. As regards the simulations of the whole combustion chamber, the average spatial discretization error of the wall heat flux is smaller because the flames of the other injectors do not penetrate into the boundary layer due to the larger distance between the injectors and the sidewall. Thus, Injector II was purposely selected among four outer injectors to estimate the maximum possible impact of the mesh.

5. Conclusions

Grid convergence studies were carried out for the flames of two selected oxygen injectors: one in the middle of the porous injector head and one near the sidewall. The CFD simulations were performed by solving the averaged Navier–Stokes equations. The numerical solution was obtained using the first-order upwind scheme for the transport equations for H and Y_i and the "High Resolution" scheme for all other variables: ρ, v_i , k, and ω. Therefore, the obtained solution is characterized by a mixed-order accuracy in space, where the solution depends both on h and on h^2. To study the dependence on the mesh spacing h, the simulations were performed on five different meshes for each injector. The meshes were generated using a global refinement/coarsening factor equal to $\sqrt[3]{2}$, so that the number of nodes was increased/decreased twice in each refinement step. The grid convergence was studied by examining two parameters: flame length and wall heat flux, which are very important as a practical matter and have the largest sensitivity to mesh spacing.

The study showed that the accuracy of the simulation results is described by a mixed order in mesh spacing, namely by a parabolic dependence on the spacing h. Therefore, at least four different meshes are required for the accurate evaluation of the order and parameters of grid convergence. In the cases of a small refinement factor, the reliable determination of convergence parameters requires even more than four meshes. The first-order and second-order terms may have a different sign, that may lead to a false feeling that the grid convergence is reached already for a coarse mesh.

On simulations of a combustion chamber with the porous injector API-68, the flames of single injectors can be simulated using the current model with a spacing of around 30 μm. As for the wall heat flux predictions, they need a very fine mesh in the region where flame interacts with boundary layer.

Acknowledgements

This work was presented at the 7th European Conference for Aeronautics and Space Sciences in Milan, Italy, 3–6 July 2017.

References

[1] J. Deeken, D. Suslov, O. Haidn, S. Schlechtriem, Combustion efficiency of a porous injector during throttling of a LOx/H_2 combustion chamber, in: L. DeLuca, C. Bonnal, O. Haidn, S. Frolov (Eds.), EUCASS Proceedings Series – Advances in AeroSpace Sciences, vol. 2, 2011, pp. 251–264.

[2] V.P. Zhukov, D.I. Suslov, Measurements and modelling of wall heat fluxes in rocket combustion chamber with porous injector head, Aerosp. Sci. Technol. 48 (2016) 67–74.

[3] V.P. Zhukov, D.I. Suslov, O.J. Haidn, CFD simulation of flow in combustion chamber with porous injector head and transpirationally cooled walls, 4th European Conference for Aerospace Sciences, 2011 paper ID: 29.

[4] V.P. Zhukov, O.J. Haidn, Analytical study of stationary temperature field in transpiration cooled porous wall, P. I. Mech. Eng. G-J. Aer. 227 (5) (2013) 873–881.

[5] ANSYS, Inc., Canonsburg, PA, USA, ANSYS CFX-solver theory guide, Release 14 (October 2012) 5.

[6] T.J. Barth, D.C. Jespersen, The design and application of upwind schemes on unstructured meshes, 27th Aerospace Sciences Meeting, Aerospace Sciences Meetings, American Institute of Aeronautics and Astronautics, Reno, NV, U.S.A., 1989.

[7] B.J. McBride, S. Gordon, Computer program for calculation of complex equilibrium compositions and applications, NASA, Tech. Rep. 1311 (1996).

[8] V.P. Zhukov, Computational fluid dynamics simulations of a GO_2/GH_2 single element combustor, J. Propul. Power 31 (6) (2015) 1707–1714.

[9] V.P. Zhukov, M. Pätz, On thermal conductivity of gas mixtures containing hydrogen, Heat Mass Transfer 53 (6) (2017) 2219–2222.

[10] G. Ribert, N. Zong, V. Yang, L. Pons, N. Darabiha, S. Candel, Counterflow diffusion flames of general fluids: oxygen/hydrogen mixtures, Combust. Flame 154 (3) (2008) 319–330.

[11] C.J. Roy, Grid convergence error analysis for mixed-order numerical schemes, AIAA J. 41 (4) (2003) 595–604.